Guided modes in the chiral negative refractive index fiber

Jianfeng Dong (董建峰)* and Jie Li (李 杰)

Institute of Optical Fiber Communication and Network Technology, Ningbo University, Ningbo 315211, China

**E-mail: dongjianfeng@nbu.edu.cn*

Received April 7, 2010

The novel characteristics of guided modes in the chiral negative refractive index fiber are investigated theoretically in this letter. We derive the characteristic equation of guided modes. Based on two types of chiral metamaterial parameters, we present the dispersion curves, energy flux, and power of guided modes. Some abnormal features, such as the existence of surface mode and dispersion curves with different shapes, intersection of dispersion curves of different guided modes, negative energy flux in the achiral cladding, and zero power at some normalized frequencies, are found in the chiral negative refractive index fiber.

OCIS codes: 060.2310, 060.2400.

doi: 10.3788/COL20100811.1032.

The negative refractive index in the chiral metamaterial has been investigated intensively in the last decade. The backward wave can propagate in the chiral metamaterial if the chirality parameter is greater than the refraction index[1−4]. A slab of such chiral metamaterial can be used as a perfect lens which providing subwavelength resolution for circularly polarized waves[5,6]. In 2009, effective negative refractive indices were realized experimentally in chiral metamaterials at microwave[7−10] and terahertz frequencies[11]. A design for chiral metamaterials with negative refractive indices at infrared frequency has also been published[12,13]. Theoretically, waveguides including chiral metamaterials with negative refractive indices have been investigated. Jin *et al.* studied the conditions for the existence of surface polariton modes on the surface of a half-space or a slab of chiral metamaterial[14]. Dong *et al.* explored the characteristics of guided and surface modes in chiral negative refractive index slab, grounded slab, and parallel-plate waveguides[15,16]. Zhang *et al.* showed that the single-mode backward wave could be guided in a planar dielectric waveguide with a strong chiral core[17]. Waves in the parallel-plate waveguide containing two-layer chiral nihility metamaterials (in which the permittivity and permeability are simultaneously zero[1]) and one air layer[18] have been examined. In our previous work, we studied the unusual characteristics of guided and surface modes in planar chiral nihility metamaterial waveguides[19,20] and chiral nihility fibers[21,22]. In this letter, we study guided modes in the chiral negative refractive index fiber. Our results are compared with the results in fibers filled with conventional chiral media (with small chirality parameters)[23,24], and in fibers[25,26] and rectangular[27] and slab[28] waveguides filled with negative index materials. Some novel characteristics are found.

Consider a chiral negative refractive index fiber whose geometry and material parameters are shown in Fig. 1. The core is an isotropic chiral metamaterial, ε_1, μ_1, κ, and the cladding is an achiral material ε_2, μ_2, (ε, μ, κ are the permittivity, permeability, and chirality parameter of the chiral medium, respectively). The radius of core is a.The cladding is assumed to extend infinitely.

The constitutive relations in an isotropic chiral medium for a time-harmonic field with $\exp(\mathrm{j}\omega t)$ can be written as[4,29]

$$\mathbf{D} = \varepsilon\mathbf{E} - \mathrm{j}\kappa\sqrt{\mu_0\varepsilon_0}\mathbf{H}, \quad \mathbf{B} = \mu\mathbf{H} + \mathrm{j}\kappa\sqrt{\mu_0\varepsilon_0}\mathbf{E}. \tag{1}$$

From the constitutive relations and Maxwell's equations, the longitudinal components of the electromagnetic fields in the core and cladding can be solved as follows[30].

In the core ($0 \le \rho \le a$):

$$\begin{cases} E_{1z} = [A_m J_m(h_{1+}\rho) + B_m J_m(h_{1-}\rho)]\exp(\mathrm{j}m\varphi) \\ H_{1z} = \frac{\mathrm{j}}{\eta_1}[A_m J_m(h_{1+}\rho) - B_m J_m(h_{1-}\rho)]\exp(\mathrm{j}m\varphi) \end{cases}; \tag{2}$$

in the cladding ($\rho \ge a$):

$$\begin{cases} E_{2z} = C_m K_m(h_2\rho)\exp(\mathrm{j}m\varphi) \\ H_{2z} = \frac{\mathrm{j}}{\eta_2} D_m K_m(h_2\rho)\exp(\mathrm{j}m\varphi) \end{cases}, \tag{3}$$

where $\exp[\mathrm{j}(\omega t - \beta z)]$ is omitted for simplicity and β is the propagation constant; $h_{1\pm} = (k_{1\pm}^2 - \beta^2)^{1/2}$, $h_2 = (\beta^2 - k_2^2)^{1/2}$, $k_{1\pm} = n_{1\pm}k_0$, $k_2 = n_2 k_0$, and $n_{1\pm} = (n_1 \pm \kappa)$ are the effective refractive indices of the right-handed circularly polarized (RCP, +) eigenwave and left-handed circularly polarized (LCP, –) eigenwave in the chiral core; $k_0 = \omega\sqrt{\mu_0\varepsilon_0}$, $n_i = \sqrt{\mu_i\varepsilon_i/\mu_0\varepsilon_0}$, and $\eta_i = \sqrt{\mu_i/\varepsilon_i}$($i$=1,2). In the chiral metamaterial, the chirality parameter is very large ($\kappa > n_1$, here we assume $\kappa > 0$), then the effective refractive index of the LCP eigenwave is negative ($n_{1-} < 0$). We call this strong chiral medium as chiral negative refractive index medium.

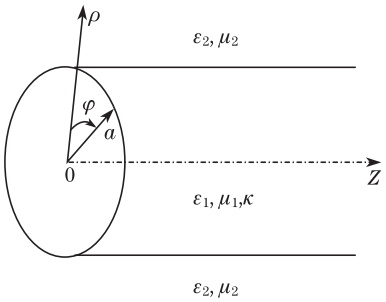

Fig. 1. Geometry and material parameters of the chiral negative refractive index fiber.

The transverse components of the electromagnetic fields $E_{1\varphi}, H_{1\varphi}, E_{2\varphi}, H_{2\varphi}$ can be derived from the relations betwwen longitudinal and transverse components of the electromagnetic fields[29]. Then, imposing the conditions of continuity of E_z, E_φ, H_z, H_φ at $\rho = a$, the characteristic equation of guided modes can be obtained as

$$a_{11}a_{22} - a_{12}a_{21} = 0, \tag{4}$$

where $a_{11} = (\frac{1}{u_+^2} + \frac{1}{v^2})m\beta a J_m(u_+) - \frac{k_{1+}a}{u_+}J'_m(u_+) - \frac{k_{2}a}{v}\frac{1}{\eta}J_m(u_+)\widehat{K}_m$, $a_{12} = (\frac{1}{u_-^2} + \frac{1}{v^2})m\beta a J_m(u_-) + \frac{k_{1-}a}{u_-}J'_m(u_-) + \frac{k_{2}a}{v}\frac{1}{\eta}J_m(u_-)\widehat{K}_m$, $a_{21} = (\frac{1}{u_+^2} + \frac{1}{v^2})m\beta a J_m(u_+) - \frac{k_{1+}a}{u_+}J'_m(u_+) - \frac{k_{2}a}{v}\eta J_m(u_+)\widehat{K}_m$, $a_{22} = -(\frac{1}{u_-^2}+\frac{1}{v^2})m\beta a J_m(u_-) - \frac{k_{1-}a}{u_-}J'_m(u_-) - \frac{k_{2}a}{v}\eta J_m(u_-)\widehat{K}_m$, and $u_\pm = h_{1\pm}a$, $v = h_2 a$, $\eta = \frac{\eta_1}{\eta_2}$, $\widehat{K}_m = \frac{K'_m(v)}{K_m(v)}$.

This characteristic equation is consistent with the results in previous studies[23,24], although the constitutive relation adopted here is different.

Energy flux along the z-axis in the waveguide is defined by

$$S_z = \frac{1}{2}\mathrm{Re}(\mathbf{E}\times\mathbf{H}^*)\cdot\hat{\mathbf{z}} = \frac{1}{2}\mathrm{Re}(E_\rho H_\varphi^* - E_\varphi H_\rho^*). \tag{5}$$

Powers in the core (P_1) and cladding (P_2) are the integration of the energy flux S_{z1} and S_{z2}, respectively:

$$P_1 = \int_0^{2\pi}\int_0^a \rho S_{z1}\mathrm{d}\rho\mathrm{d}\varphi = 2\pi\int_0^a \rho S_{z1}\mathrm{d}\rho, \tag{6a}$$

$$P_2 = \int_0^{2\pi}\int_a^\infty \rho S_{z2}\mathrm{d}\rho\mathrm{d}\varphi = 2\pi\int_a^\infty \rho S_{z2}\mathrm{d}\rho. \tag{6b}$$

The normalized power is defined as[25]

$$P = \frac{P_1 + P_2}{|P_1| + |P_2|}. \tag{7}$$

Now we present the numerical results for two types of chiral metamaterial parameters that both satisfy $n_2 < |n_{1-}| < n_{1+}$: $n_1 > n_2$ and $n_1 < n_2$. Here we use normalized frequency $V = k_0 a\sqrt{|n_1^2 - n_2^2|}$ because the chiral metamaterial occurs only at a certain frequency.

Consider the first case: $n_1 > n_2$. We choose $\varepsilon_1 = 2.25\varepsilon_0$, $\mu_1 = \mu_0$, $\varepsilon_2 = \varepsilon_0$, $\mu_2 = \mu_0$, and $\kappa = 2.6$, and refractive index parameters $n_{1+} = 4.1$, $n_{1-} = -1.1$, $n_1 = 1.5$, and $n_2 = 1.0$, which satisfy $n_{1-} < 0$ (chiral negative refractive index), $n_1 > n_2$, and $n_2 < |n_{1-}| < n_{1+}$.

Figure 2 shows the normalized propagation constant β/k_0 versus normalized frequency V for modes (a) m=0, (b) m=–1,1, and (c) m=–2,2, in the chiral negative refractive index fiber for $n_1 > n_2$. Solid curves correspond to m= 0, –1, –2 and dashed curves correspond to m=1, 2, where H_{mn} and H_{ms} stand for guided modes and surface modes, respectively.

Figure 2 shows some novel characteristics of dispersion curves as follows.

1) Mode bifurcation (i.e., propagation constants are different for different signs of m). The cutoff frequencies

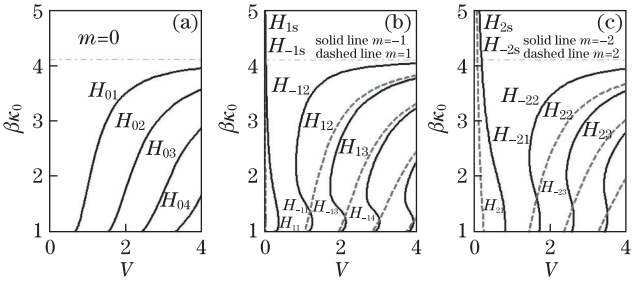

Fig. 2. Dispersion curves of modes in the chiral negative refractive index fiber for $n_1 > n_2$ (a) m=0; (b) m=–1, 1; (c) m=–2, 2.

of m=–1,1 guided modes are the same, which satisfy the equation $J_1(\sqrt{k_{1+}^2 - k_2^2}a) = 0$. However, the cutoff frequencies of m=–2,2 guided modes are different. The mode bifurcation phenomenon occurs in the conventional chiral fibers (with small chirality parameters)[23,24]; however, it cannot occur in negative refractive index fibers[25,26].

2) Dispersion curves of m=–1, –2 guided modes are bent, with their shapes similar to the letter "S" for the second- and other higher-order guided modes. In some range of V, there are two or three values of propagation constants for a fixed V, and the slope of dispersion curves can be negative. Similar dispersion curves can be found in negative refractive index fibers[25]. In the conventional chiral fibers[23,24], the slopes of dispersion curves are always positive.

3) There are several mode intersections, such as those in guided modes of H_{-12} and H_{12}, H_{-13} and H_{13}, H_{-22} and H_{22}, H_{-23} and H_{23}, and so on. These modes have same propagation constant (mode matching or perfect phase matching) at the crossing point. Generally, mode matching can be realized in anisotropic waveguides and can be applied for efficient fiber-to-planar waveguide coupling, mode filtering, and improvement of mode conversion efficiency[25]. Mode intersection also occurs in conventional chiral fibers[24] and negative refractive index fibers[25].

4) Surface modes exist for m=–1, 1, –2, 2. Surface modes connect continuously to the first guided modes at the crossing point of dashdotted (corresponding to n_{1+}) and solid or dashed curves. The slopes of dispersion curves of surface modes are negative (i.e., the normalized propagation constant β/k_0 increases monotonoically as the normalized frequency V decreases). The slope of the curves of H_{11} and H_{21} guided modes and H_{1s}, H_{2s} surface modes are very steep, which may have potential application in high-sensitivity optical sensor in the future. Surface modes have been previously found in fiber[25,26], as well as rectangular[27] and slab[28] waveguides, filled with negative index materials.

In the conventional chiral fiber, the energy flux S_z in the cladding is positive and decays exponentially from the interface between the core and cladding. However, there are exotic features for H_{11} and H_{1s} modes (and H_{21}, H_{2s} modes) in the chiral negative refractive index fiber. The energy flux S_z is negative in the cladding and positive in the core. This phenomenon has also been found in chiral nihility fiber[21]; however, it has not been found in

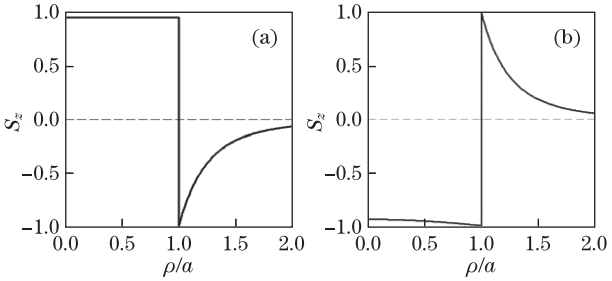

Fig. 3. Energy flux S_z for H_{11} and H_{-11} guided modes. (a) H_{11} mode, V=0.05, β/k_0=2.2606; (b) H_{-11} mode, V=0.35, β/k_0=1.4735.

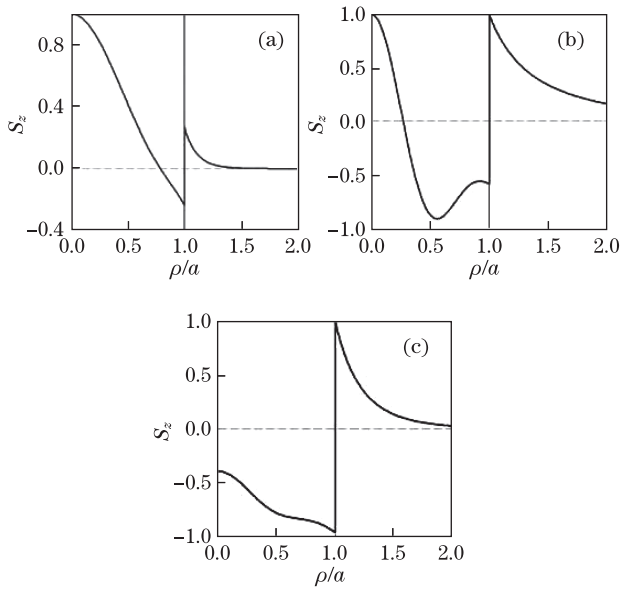

Fig. 4. Energy flux S_z of three propagation constants at V=1.25 for H_{-12} guided mode. (a) β/k_0=3.4638; (b) β/k_0=1.0487; (c) β/k_0=1.3337.

the chiral metamaterial slab[14], grounded slab[15,16], and negative refractive index fibers[25]. Figure 3(a) shows the energy flux S_z at normalized frequency V=0.05 for H_{11} guided mode. The energy flux S_z is almost a constant in the core. For comparison, Fig. 3(b) shows the energy flux S_z at normalized frequency V= 0.35 for H_{-11} guided mode. In both Figs. 3(a) and (b), the energy flux is in opposite directions in the core and cladding. The normalized power is negative at V= 0.05 for H_{11} guided mode and V= 0.35 for H_{-11} guided mode; therefore, they are backward waves. Furthermore, the normalized powers of all surface and guided modes are always negative in the region of negative slope of dispersion curves, as shown in Fig. 2.

There are three propagation constants for H_{-12}, H_{-13}, and other higher-order guided modes for a fixed V. The distributions of energy flux S_z are different for different propagation constants. The energy flux S_z at normalized frequency V=1.25 for H_{-12} guided mode is shown in Fig. 4. For a larger propagation constant β/k_0=3.4638 (Fig. 4(a)) and a smaller propagation constant β/k_0=1.0487 (Fig. 4(b)), the energy flux S_z is negative near the interface between the core and cladding, and positive near the center of the core. Change in sign of the energy flux within the negative refractive index region has also been found in the chiral nihility fiber[21] and

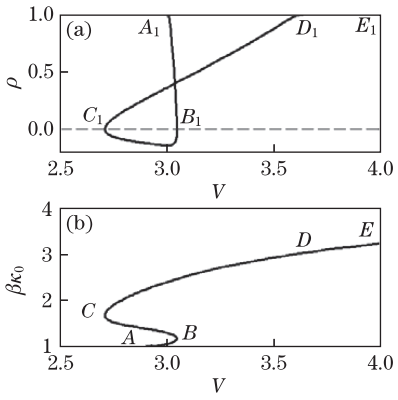

Fig. 5. (a) Normalized power P versus normalized frequency V for H_{-14} guided mode; (b) dispersion curve of H_{-14} guided mode.

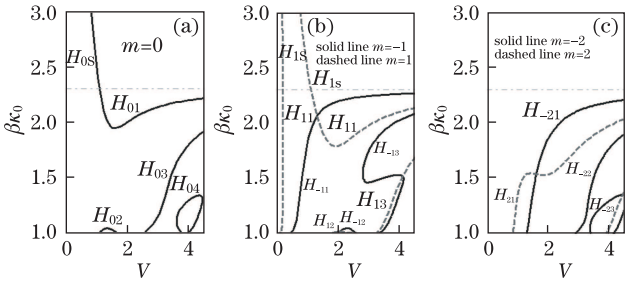

Fig. 6. Dispersion curves of modes in the chiral negative refractive index fiber for $n_1 < n_2$. (a)m=0; (b)m=–1, 1; (c)m=–2, 2.

negative refractive index fiber[26]. For a middle propagation constant β/k_0=1.3337 (Fig. 4(c)), the energy flux S_z is always negative in the core. The normalized power is positive for larger and smaller propagation constants, and negative for a middle propagation constant.

The characteristics of normalized power P for H_{-12}, H_{-13}, and other higher-order guided modes are similar. Figure 5(a) shows the normalized power P versus normalized frequency V for H_{-14} guided mode. The dispersion curve is also plotted in Fig. 5(b) in order to demonstrate clearly. For larger V, the normalized power is equal to 1 (region E_1D_1or ED). P decreases from 1 to 0 as V decreases to the lowest limiting frequency, which corresponds to actual cutoff of H_{-14} guided mode (region E_1C_1 or DC). In the region of negative slope of the dispersion curve (region C_1B_1 or CB), P is negative. Then, P increases to 1 in the region of positive slope of dispersion curve at smaller propagation constant (region B_1A_1 or BA). Interestingly, the power P at points B_1 and C_1 is equal to zero, corresponding to zero group velocity. This implies that at these points, the waveguide cannot propagate energy, i.e., it would be able to halt the light. Waves with this feature are of great practical interest for optical communication and data storage applications.

Now we consider the second case: $n_1 < n_2$. If we choose $\varepsilon_1 = 0.09\varepsilon_0$, $\mu_1 = \mu_0$, $\varepsilon_2 = \varepsilon_0$, $\mu_2 = \mu_0$, and $\kappa = 2.0$, then refractive index parameters $n_{1+} = 2.3$, $n_{1-} = -1.7$, $n_1 = 0.3$, and $n_2 = 1.0$, which satisfy $n_{1-} < 0$ (chiral negative refractive index), $n_1 < n_2$, and $n_2 < |n_{1-}| < n_{1+}$.

Although $n_1 < n_2$, guided modes can exist in the chiral negative refractive index fiber because the chiral negative refractive index fiber core behaves as a combined medium of two media with effective index $n_{1+} = 2.3$, and $n_{1-} = -1.7$, respectively. The absolute values of effective index are greater than 1; thus, total internal reflection can occur at the interface between the chiral negative refractive index fiber core and air cladding. Figure 6 shows the normalized propagation constant β/k_0 versus normalized frequency V for modes in the chiral negative refractive index fiber for $n_1 < n_2$. Apart from mode bifurcation and intersection, "S" shape dispersion curve, and surface modes, as discussed in the case of $n_1 > n_2$, some other abnormal characteristics can be found from Fig. 6.

1) Shapes of dispersion curves of H_{01} and H_{11} guided modes look similar to the letter "L".

2) H_{02}, H_{12}, and H_{-12} guided modes have two cutoff frequencies (i.e., these guided modes exist in the region between two normalized cutoff frequencies). This phenomenon has not been found in negative refractive index fibers[25].

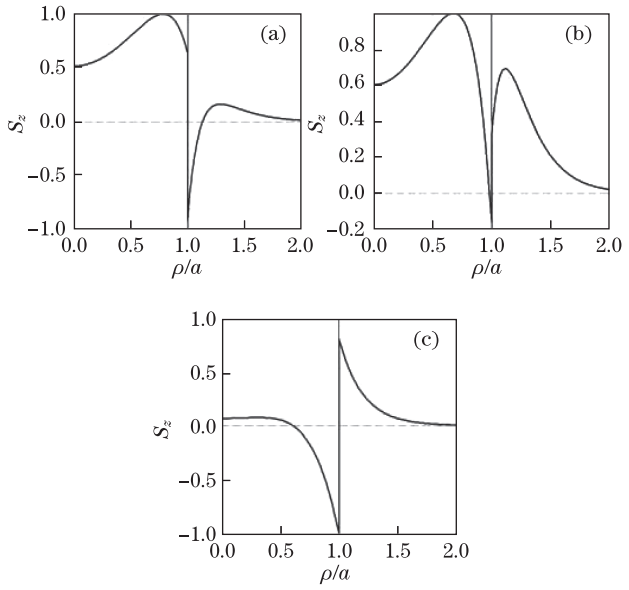

Fig. 7. Energy flux S_z at different V for H_{1s} andH_{11} modes. (a)H_{1s} mode, V=0.7, β/k_0=3.2791; (b)H_{1s} mode, V=0.8, β/k_0=2.9662; (c)H_{11} mode, V=1.5, β/k_0=1.9229.

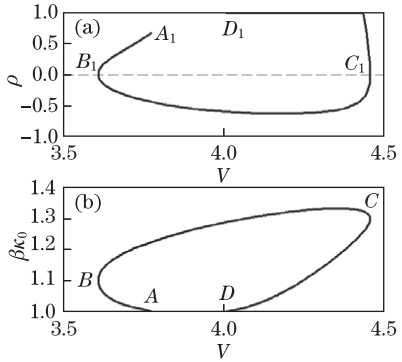

Fig. 8. (a) Normalized power P versus normalized frequency V for H_{04} guided mode; (b) dispersion curve of H_{04} guided mode

3) The shape of dispersion curve of H_{04} guided mode is elliptical.

Figure 7 shows the energy flux S_z at different normalized frequency V for H_{1s} and H_{11} modes. For H_{1s} surface mode, at V=0.7, the energy flux S_z in the core is positive, while the energy flux S_z in the cladding is negative near the interface and positive, away from the interface. For H_{1s} surface mode, at V=0.8, the energy flux S_z in the core is positive near the center of the core and negative near the interface, while the energy flux S_z in the cladding is positive. For H_{11} guided mode, at V=1.5, the energy flux S_z in the core is positive near the center of the core and negative near the interface, and positive in the cladding. However, the absolute value of energy flux S_z is the largest at the interface. For all these cases, the normalized power is positive, and the modes are forward waves.

Figure 8 shows the normalized power P versus the normalized frequency V for H_{04} guided mode; dispersion curve is also plotted. In the regions of AB and CD in the dispersion curve, P is positive (regions A_1B_1 and C_1D_1). In the region of BC in dispersion curve, P is negative (region B_1C_1). In addition, the power P at points B_1 and C_1 is equal to zero, corresponding to zero group velocity.

The abnormal results for two cases discussed above stem from the behavior of the chiral negative refractive index fiber core as a combined medium of two media with effective index $n_{1-}(n_{1-} < 0$, negative index material) and $n_{1+}(n_{1+} > 0$, conventional material). In the negative index material, the wave vector propagation is anti-parallel with the energy flux; in the conventional material, the wavevector propagation is parallel with the energy flux. In addition, the absolute value of $n_{1\pm}$ is larger than the refractive index of cladding. As a result, complex characteristics of guided mode in the chiral negative refractive index fiber emerge.

The characteristics of guided modes in the chiral negative refractive index fiber that consists of a chiral metamaterial core with an achiral cladding have been investigated theoretically in this letter. We obtain the characteristic equation of guided modes. We plot and present the dispersion curves, energy flux, and power of several low-order guided modes for two type chiral metamaterials parameters. Some novel features are found in the chiral negative refractive index fiber, such as the existence of surface mode and dispersion curves with different abnormal shape, intersection of dispersion curves of different guided modes, negative energy flux in the achiral cladding, and zero power at some normalized frequencies. Some of these characteristics have also been found in the negative refractive index fiber. However, some characteristics, such as negative energy flux in the achiral cladding, mode bifurcation, and guided modes that exist in the region between two normalized cutoff frequencies, have not been found in the negative refractive index fiber. The results presented here will be helpful for potential applications in new fiber devices.

This work was supported by the Natural Science Foundation of Zhejiang Province (No. Y1091139) and partially sponsored by the K. C. Wong Magna Fund in Ningbo University.

References

1. S. Tretyakov, I. Nefedov, A. Sihvola, S. Maslovski, and C. Simovski, J. Electromagn. Waves Appl. **17,** 695 (2003).
2. J. B. Pendry, Science **306,** 1353 (2004).
3. T. G. Mackay, Microwave Opt. Tech. Lett. **45,** 120 (2005).
4. S. Tretyakov, A. Sihvola, and L. Jylhä, Photon. Nanostruct. **3,** 107 (2005).
5. C. Monzon and D. W. Forester, Phys. Rev. Lett. **95,** 123904 (2005).
6. Y. Jin and S. He, Opt. Express **13,** 4974 (2005).
7. E. Plum, J. Zhou, J. Dong, V. A. Fedotov, T. Koschny, C. M. Soukoulis, and N. I. Zheludev, Phys. Rev. B **79,** 035407 (2009).
8. J. Zhou, J. Dong, B. Wang, T. Koschny, M. Kafesaki, and C. M. Soukoulis, Phys. Rev. B **79,** 121104 (2009).
9. B. Wang, J. Zhou, T. Koschny, and C. M. Soukoulis, Appl. Phys. Lett. **94,** 151112 (2009).
10. M. C. K. Wiltshire, J. B. Pendry, and J. V. Hajnal, J. Phys.: Condens. Matter **21,** 292201 (2009).
11. S. Zhang, Y. Park, J. Li, X. Lu, W. Zhang, and X. Zhang, Phys. Rev. Lett. **102,** 023901 (2009).
12. D. Kwon, D. H. Werner, A. V. Kildishev, and V. M. Shalaev, Opt. Express **16,** 11822 (2008).
13. J. Dong, J. Zhou, T. Koschny, and C. M. Soukoulis, Opt. Express **17,** 14172 (2009).
14. Y. Jin, J. He, and S. He, Phys. Lett. A **351,** 354 (2006).
15. J. F. Dong, Prog. Electromagn. Res. **95,** 153 (2009).
16. J. F. Dong, Z. J. Wang, L. L. Wang, and B. Liu, in *Proceedings of International Symposium on Biophotonics, Nanophotonics and Metamaterials* 517 (2006).
17. C. Zhang and T. J. Cui, Opt. Commun. **280,** 359 (2007).
18. Q. Cheng and C. Zhang, Opt. Commun. **276,** 317 (2007).
19. J. Dong and C. Xu, Prog. Electromagn. Res. B **14,** 107 (2009).
20. J. F. Dong and C. Xu, Opt. Commun. **282,** 3899 (2009).
21. J. Dong, Prog. Electromagn. Res. **99,** 163 (2009).
22. J. F. Dong, Opt. Commun. **283,** 532 (2010).
23. R. C. Qiu and I.-T. Lu, J. Opt. Soc. Am. A **11,** 3212 (1994).
24. S. F. Mahmoud, IEEE Trans. Microwave Theory Tech. **43,** 205 (1995).
25. A. V. Novitsky and L. M. Barkovsky, J. Opt. A: Pure Appl. Opt. **7,** S51 (2005).
26. K. Y. Kim, J. H. Lee, Y. K. Cho, and H. S. Tae, Opt. Express **13,** 3653 (2005).
27. Z. Wang, J. Zhou, L. Zhang, H. Ren, and C. Jin, Acta Opt. Sin. (in Chinese) **28,** 1558 (2008).
28. J. Zhang, Y. He, C. Li, and F. Zhang, Acta Opt. Sin. (in Chinese) **29,** 2673 (2009).
29. I. V. Lindell, A. H. Sihvola, S. A. Tretyakov, and A. J. Viitanen, *Electromagnetic Waves in Chiral and Bi-Isotropic Media* (Artech House, Boston, 1994).
30. J. Dong, W. Tao, and J. Xu, Acta Photon. Sin. (in Chinese) **36,** 1044 (2007).